arXiv:1610.07358v1 [cond-mat.mes-hall] 24 Oct 2016

Electrically tunable artificial gauge potential for polaritons

Hyang-Tag Lim*, Emre Togan*, Martin Kroner, Javier Miguel-Sanchez, and Atac Imamoğlu

Institute of Quantum Electronics, ETH Zurich, CH-8093 Zurich, Switzerland.

* *These authors contributed equally to this work.*

Neutral particles subject to artificial gauge potentials can behave as charged particles in magnetic fields. This fascinating premise has led to demonstrations of one-way waveguides, topologically protected edge states and Landau levels for photons. In ultracold neutral atoms effective gauge fields have allowed the emulation of matter under strong magnetic fields leading to realization of Harper-Hofstadter and Haldane models. Here we show that application of perpendicular electric and magnetic fields effects a tuneable artificial gauge potential for two-dimensional microcavity exciton polaritons. For verification, we perform interferometric measurement of the associated phase accumulated during coherent polariton transport. Since the gauge potential originates from the magnetoelectric Stark effect, it can be realized for photons strongly coupled to excitations in any polarizable medium. Together with strong polariton-polariton interactions and engineered polariton lattices, artificial gauge fields could play a key role in investigation of non-equilibrium dynamics of strongly correlated photons.

Synthesis of artificial gauge fields for photons have been demonstrated in a number of different optical systems. In most cases, the implementation is achieved through the design of the optical system [1–4], leaving little or no room for fast control of the magnitude of the effected gauge field after sample fabrication is completed. For many applications on the other hand, it is essential to be able to tune or adjust the strength of the gauge field during the experiment [5–7]; this is particularly the case for nanophotonic structures [8] where fast local control of the gauge field strength may open up new possibilities for investigation of many-body physics of light [9]. The realization we describe here has the potential to fulfill this premise since the strength and direction of the effected gauge potential is controlled electrically. Moreover, since our scheme relies on the magnetoelectric Stark effect, time reversal symmetry [10–12] of the optical excitations is broken.

Cavity-polaritons are hybrid light-matter quasi-particles arising from non-perturbative coupling

between quantum well (QW) excitons and cavity photons. A magnetic field B_z applied along the growth direction influences polaritons through their excitonic nature and leads to a diamagnetic shift, Zeeman splitting of circularly polarized modes and enhancement of exciton-photon coupling strength [13]. For excitons with a non-zero momentum, the applied B_z also induces an electric dipole moment [14–17]. In a classical picture, this dipole moment is due to the Lorentz force that creates an effective electric field E_{eff} [18] that is proportional to $\vec{k} \times \vec{B}$. For excitons with small momentum and polarizability α, this E_{eff} causes an induced dipole moment ($\vec{d} \propto \alpha \vec{k} \times \vec{B}$). An additional external electric field $\vec{E}_{\text{ext}}$ in the QW plane then alters the dispersion of excitons as it leads to energy changes proportional to k: $-\vec{d} \cdot \vec{E}_{\text{ext}} \propto -\alpha \left(\vec{k} \times \vec{B}\right) \cdot \vec{E}_{\text{ext}}$, so that the energy minimum is no longer at $|\vec{k}| = 0$ as would be the case for a free particle with an effective mass but at finite $\vec{k}$. This simple modification of the dispersion relation is equivalent to an effective gauge potential A_{eff} for excitons; due to their partly excitonic character, the hamiltonian describing the dynamics of polaritons also contains a term proportional to A_{eff}.

We first demonstrate the presence of an effective electric field whose magnitude and direction depends on the direction of propagation for polaritons subjected to an out-of-plane magnetic field. The cavity polariton sample we use is illustrated in Figure 1a. Our demonstration relies on the fact that it is possible to excite polaritons with a well defined in-plane wavevector $\vec{k}$ by appropriately choosing the angle and energy of the excitation beam. As illustrated in Figure 1a we choose $\vec{k} = k_y \hat{y}$. Two metal gates deposited 30 μm apart allow us to apply an electric field in the x direction such that for polaritons propagating with a wavevector along the y direction, $\vec{E}_{\text{ext}}$ will add or cancel E_{eff} due to the Lorentz force. By recording changes in the transition energy of polaritons as a function of E_{ext} we can determine the strength of E_{eff}. In our experiments, we only address the lower polariton branch.

Changes in the reflected intensity of a laser beam probing polaritons at $B_z = 0$ T with $k_y^+ = 2.7\ \mu\text{m}^{-1}$ as a function of E_{ext} is shown in Figure 1d. For each E_{ext} the reflected intensity shows a dip at an energy corresponding to the polariton resonance (Figure 1e). The spectral center of the dip shifts to lower energies with E_{ext} in a way that is well described by a second order polynomial. The expected behaviour for a neutral polarizable quasi-particle (i.e. exciton or polariton) that is subject to E_{ext}, would be to have a dc-Stark shift proportional to $-\alpha \left|E_{\text{ext}}\right|^2$ [19]; here, the coefficient α is the quasi-particle polarizability. Therefore the electric field that yields the maximum lower polariton energy identifies $E_{\text{ext}} = \tilde{E}_{\text{ext}}$ that exactly cancels any internal or effective electric fields

E_{eff} ($\tilde{E}_{\text{ext}} = -E_{\text{eff}}$). To quantify E_{eff} due to the Lorentz force described above, we extract the difference of $\tilde{E}_{\text{ext}}$ at a fixed B_z for polaritons excited with $k_y^+ = 2.7\ \mu\text{m}^{-1}$ and $k_y^- = -2.9\ \mu\text{m}^{-1}$. This approach also allows us to exclude influences of built in electric fields. At $B_z = 0$ T we find that the difference of V_G values that correspond to the maximum energy with $k_y^{\pm}$ excitation is 0.02 V, indicating that E_{eff} is negligible at 0 T (Figure 1f).

In stark contrast, for $B_z = 5$ T the energy shift of polaritons with E_{ext} displays a significant difference between $\tilde{E}_{\text{ext}}$ for k_y^+ and k_y^-, as illustrated in Figure 2a. Magnetic field dependence of the difference of $\tilde{E}_{\text{ext}}$ for $k_y^{\pm}$, Figure 2b, shows a behaviour that is well described by a linear increase with B_z, demonstrating E_{eff} due to the Lorentz force.

The shape of the parabolas also contain further information about the B_z induced changes to the polaritons. With increasing B_z, the polarizability decreases and the polariton energy at $E_{\text{ext}} = 0$ increases, as illustrated in Figure 2c. The polariton energy at $E_{\text{ext}} = 0$ and the polarizability can be extracted from a fit to a second order polynomial: $\epsilon_0 - \vec{d} \cdot \vec{E}_{\text{ext}} - \alpha E_{\text{ext}}^2$. The first order coefficient of the polynomial in turn, yields the induced dipole moment of the polaritons (excitons). The difference of the first order coefficient for $\pm k_y$ excitation beams (twice the induced dipole moment) are shown in Figure 2d: we observe that the induced dipole moment first increases with B_z and then starts to slowly decrease for $B_z \geq 4$ T. We expect that for the high magnetic field regime, the induced dipole moment decreases as $\left|\vec{d}\right| \sim 1/B_z$ [15]. We find very good agreement with a theoretical model of the polaritons (shown as solid lines in Figure 2) that allows us to identify the physical mechanism underlying the overall B_z and E_{ext} dependence (see Supplementary Information for the detailed information about the model). The change in the lower polariton energy is due to an interplay between a diamagnetic blue shift of the exciton transition energy and a red-shift due to an increase in the cavity-exciton coupling strength [13]. Concurrently, the polarizability decreases with B_z, as would be expected in a classical picture as the size of the polarizable particle decreases. We emphasize that due to the change in the exciton energy and cavity-exciton coupling strength the exciton content of the polaritons changes as B_z is varied. We also find that the energy shift of polaritons with E_{ext} is influenced by the decrease in the electron hole overlap due to E_{ext} induced polarization, which leads to a reduction of the cavity-exciton coupling strength. In the E_{ext} range that we probe the decrease in the cavity-exciton coupling leads to an effective smaller polarizability for polaritons as compared to excitons, due to a reduction on the excitonic character of the polaritons. Moreover, the model also captures the presence of E_{eff} due to the center of

mass motion of polaritons and confirms that even with changes in exciton content with B_z, its expected dependence on B_z is still linear. Finally, we emphasize that while E_{eff} arises from exciton physics, the strong coupling between excitons and photons has to be taken into account to obtain a quantitative agreement between the model and our experiments.

Remarkably, our findings demonstrate that polariton energy under perpendicular B_z and E_{ext} depends not only on the magnitude of k_y but also on its direction: this non-reciprocal flow of light is an indication of the presence of a gauge field for polaritons. The dispersion relation for free excitons propagating in the QW plane with wavevector $k_y\hat{y}$ in the presence of an electric field $\vec{E} = (\frac{\hbar}{M}k_y B_z + E_{\text{ext}})\hat{x}$ is:

$$\epsilon_{\text{exc}}(k_y) = \epsilon_{\text{exc}}(0) + \frac{\hbar^2 k_y^2}{2M} - \alpha\left(\frac{\hbar}{M}k_y B_z + E_{\text{ext}}\right)^2 = \epsilon'_{\text{exc}} + \frac{(\hbar k_y - qA_{\text{eff}})^2}{2M'}, \tag{1}$$

where M is the total exciton mass, and $\epsilon_{\text{exc}}(0)$ is the exciton energy at $k_y = 0$ and $E_{\text{ext}} = 0$. $qA_{\text{eff}} = \frac{M'}{M}2\alpha B_z E_{\text{ext}}$ is an effective vector potential for excitons, with $\epsilon'_{\text{exc}} = \epsilon_{\text{exc}}(0) - \alpha E_{\text{ext}}^2 - \frac{(qA_{\text{eff}})^2}{2M'}$ and $M' = M\left(1 - \frac{\alpha B_z^2}{2M}\right)^{-1}$. The strong coupling to the cavity further changes the dispersion relation, but, polaritons in a narrow energy-momentum range can still be treated as free particles under the influence of qA, whose value depends on the detuning between the excitons and polaritons as well as their effective masses (see Supplementary Information).

For our experiments both B_z and E_{ext} are uniform over the area of our experiment yielding a constant gauge potential qA. Since physical observables are gauge invariant, we might expect our measurements to be independent of qA. In practice, our experiments involve propagation of photons between two regions with different constant gauge potentials; when calculating the magnitude of qA above, we fixed a gauge by choosing the constant gauge potential for photons outside the cavity to be $qA = 0$. Conversely, qA is observable in our experiments due to the presence of an effective (sheet) magnetic field at the interface between the cavity and vacuum that imparts kicks to the canonical momentum as photons/polaritons pass through the interface [20].

To demonstrate the validity of the description of photon/polariton dynamics as determined by a gauge potential, we perform an interference experiment where we measure the phase accumulated by polaritons propagating for a length l inside the sample relative to a fixed phase reference (see Figure 3a and Methods for detailed information about the interference experiment). An interference image obtained at $E_{\text{ext}} = 0$ is shown in Figure 3b. Changes in the interference pattern with y at two different E_{ext} are illustrated in Figure 3c.

A plot of the phase change of polaritons with $E_{\rm ext}$ for different direction of excitation at $B_z = 6$ T is shown in Figure 3d. The data shows that at a fixed $E_{\rm ext}$ and at the same excitation frequency, the phase accumulated for polaritons propagating along $\pm\hat{y}$ directions differ, and that this phase difference depends on the sign of $E_{\rm ext}$ and B_z. The in-plane momentum of the polaritons with a fixed energy is modified by the absence or presence of a constant vector potential so that the additional accumulated phase for traveling a distance l is given by $\frac{q}{\hbar}\int \vec{A}\cdot dl$. At a fixed $E_{\rm ext}$ the difference between the phase accumulated when exciting with $k_y^{\pm}$ allows us to avoid phase changes due to the Stark effect and to directly obtain $\Delta\phi_{k_y^+} - \Delta\phi_{k_y^-} = 2\frac{q}{\hbar}Al$. The fact that $\Delta\phi_{k_y^+} - \Delta\phi_{k_y^-}$ depends both on the sign of the electric field as well as the magnetic field is another manifestation of the validity of the description with $A^{\rm eff}$. Since the phase shift as a function of $E_{\rm ext}$ can be modeled with a second order polynomial in $E_{\rm ext}$, the dc-Stark effect is the dominant underlying mechanism for the phase shift. Figure 3d shows that polaritons acquire a phase shift of ~ 0.25 radians due to qA as they propagate an average distance $l = 9\,\mu$m. Hence, the parameters of our experiment already ensure significant phase accumulation over the lattice constant ($\geq 2.4\,\mu$m) of state of the art polariton lattices [8] or average seperation ($\sim 4\,\mu$m) of coupled polariton microcavities [21]. Choosing detunings that yield predominantly exciton-like lower polaritons will further increase qA. In addition, employing structures with longer polariton lifetimes [22] will allow the realization of polariton lattices with larger lattice constants. With these advances, it should be possible to design structures where accumulated polariton phase due to qA in a unit cell could be on the order of π.

Together with strong photon-photon interactions, realization of tunable artificial gauge fields is key for ongoing research aimed at observation of topological order in driven-dissipative photonic systems [23, 24]. Cavity-polaritons constitute particularly promising candidates in this endeavour since their partly exciton nature enhances interactions [25–27] and ensures time-reversal-symmetry breaking by external magnetic fields [28, 29]. Our work demonstrates that the same polariton system also allows for realization of tunable gauge fields, if an in-plane electric-field gradient is introduced in the QW. While such gradients are manifest in most gated structures, creation of a constant artificial magnetic field over a region of several μm should be possible in specially designed structures. We envision that lattices of dipolaritons [30] would provide a very promising avenue towards this endeavour: the use of an in-plane magnetic field in this case would effect a gauge potential that is substantially enhanced by the large dipolariton-polarizability and strong external electric fields along the growth direction [16, 17]. The gradients of the latter in turn

could be used to generate fluxes approaching magnetic flux quantum in a plaquette of area $\sim 5 \times 5 \mu m^2$. (Di)Polaritons subject to complex electric field distributions enabling large, tunable and inhomogeneous effective gauge field profiles [31] would constitute a novel feature in exploration of topologically non-trivial non-equilibrium quantum systems.

I. METHODS

In-plane electric field. As described in Figure 1a, we apply an electric potential V_G between two gates to create E_{ext}. We find a good agreement between our data and a numerical calculation for the polariton behavior (see Supplementary Information) with the electric field $E_{\text{ext}} = 0.84\ V_G/(30\,\mu\text{m})$. Since the two quantities are linearly related we use E_{ext} and V_G interchangeably. For all experiments that involve a non-zero in-plane electric field, we acquire data in a pulse sequence (see Supplementary Information). This sequence is applied in order to avoid charge accumulation induced variation in the actual electric field.

Polariton interference measurement. We use the setup depicted in Figure 3a to create two beams that are incident with different in plane momenta ($k_y^{\pm}$ and $k = 0$) and are separated by l. The laser energy is chosen to be nearly resonant with the polariton modes with $k_y^{\pm}$. Thanks to the steep polariton dispersion, at the same energy, $k = 0$ beam is off resonance from the polariton modes; the photons in this beam are therefore reflected by the top mirror without being subject to A^{eff}. Photons in the $k_y^{\pm}$ beam are converted into a propagating polariton cloud. As polaritons propagate towards the position of the $k = 0$ beam, they accrue an additional phase due to A^{eff}. Propagating polaritons continue to emit photons out of the sample, and when these photons overlap with those from the $k = 0$ beam they interfere, allowing us to measure changes in the accumulated phase.

We model the light intensity in the region where the interference occurs (interference region) as the sum of a Gaussian ($k = 0$ beam) and a plane wave (polaritons propagating with k_y):

$$|b_0 e^{-(y-y_0)^2/\sigma_y^2} + a_0 e^{i\phi} e^{-ik_y y}|^2 + b_1.$$

We independently determine b_0, σ_y, and y_0 using images obtained at very high applied electric field for which the polariton term is negligible ($a_0 \ll b_0$), and fix k_y. For each E_{ext} we fit for a_0, b_1, and ϕ values.

Since our excitation beams have a finite size, they have a finite width in k_y ($0.45\ \mu\mathrm{m}^{-1}$), therefore the exact k_y value of the polaritons that are excited is determined by the energy of the excitation beam. For a fixed excitation laser energy, changes in E_{ext} will shift the dispersion relation so that $k_y + \Delta k_y$ is resonant with the excitation laser. These changes (due to A^{eff} or Stark effect) in the dispersion relation show up as phase changes in our experiments, $\Delta\phi = l\Delta k_y$ where l is the mean distance from the excitation spot to the interference region. Since we are interested in how the phase changes with E_{ext} and the absolute phase between the two beams is not determined, we set the phase at $E_{\mathrm{ext}} = 0$ to 0 radian.

---

[1] Rechtsman, M. C. *et al.* Strain-induced pseudomagnetic field and photonic Landau levels in dielectric structures. *Nature Photonics* **7**, 153–158 (2012).

[2] Rechtsman, M. C. *et al.* Photonic Floquet topological insulators. *Nature* **496**, 196–200 (2013).

[3] Hafezi, M., Mittal, S., Fan, J., Migdall, A. & Taylor, J. M. Imaging topological edge states in silicon photonics. *Nature Photonics* **7**, 1001–1005 (2013).

[4] Schine, N., Ryou, A., Gromov, A., Sommer, A. & Simon, J. Synthetic Landau levels for photons. *Nature* **534**, 671–675 (2016).

[5] Aidelsburger, M. *et al.* Realization of the Hofstadter hamiltonian with ultracold atoms in optical lattices. *Physical Review Letters* **111**, 185301 (2013).

[6] Jotzu, G. *et al.* Experimental realization of the topological Haldane model with ultracold fermions. *Nature* **515**, 237–240 (2014).

[7] Dalibard, J., Gerbier, F., Juzelinas, G. & Öhberg, P. Colloquium: Artificial gauge potentials for neutral atoms. *Reviews of Modern Physics* **83**, 1523–1543 (2011).

[8] Jacqmin, T. *et al.* Direct observation of Dirac cones and a flatband in a honeycomb lattice for polaritons. *Physical Review Letters* **112**, 116402 (2014).

[9] Carusotto, I. & Ciuti, C. Quantum fluids of light. *Reviews of Modern Physics* **85**, 299–366 (2013).

[10] Wang, Z., Chong, Y., Joannopoulos, J. D. & Soljacic, M. Observation of unidirectional backscattering-immune topological electromagnetic states. *Nature* **461**, 772–775 (2009).

[11] Fang, K., Yu, Z. & Fan, S. Realizing effective magnetic field for photons by controlling the phase of dynamic modulation. *Nature Photonics* **6**, 782–787 (2012).

[12] Tzuang, L. D., Fang, K., Nussenzveig, P., Fan, S. & Lipson, M. Non-reciprocal phase shift induced by an effective magnetic flux for light. *Nature Photonics* **8**, 701–705 (2014).

[13] Pietka, B. *et al.* Magnetic field tuning of exciton-polaritons in a semiconductor microcavity. *Physical*

Review B **91**, 075309 (2015).

[14] Kallin, C. & Halperin, B. I. Excitations from a filled Landau level in the two-dimensional electron gas. *Physical Review B* **30**, 5655–5668 (1984).

[15] Paquet, D., Rice, T. M. & Ueda, K. Two-dimensional electron-hole fluid in a strong perpendicular magnetic field: Exciton Bose condensate or maximum density two-dimensional droplet. *Physical Review B* **32**, 5208–5221 (1985).

[16] Lozovik, Y. E., Ovchinnikov, I. V., Volkov, S. Y., Butov, L. V. & Chemla, D. S. Quasi-two-dimensional excitons in finite magnetic fields. *Physical Review B* **65**, 235304 (2002).

[17] Butov, L. V. *et al.* Observation of magnetically induced effective-mass enhancement of quasi-2d excitons. *Physical Review Letters* **87**, 216804 (2001).

[18] Thomas, D. G. & Hopfield, J. J. A magneto-Stark effect and exciton motion in CdS. *Physical Review* **124**, 657–665 (1961).

[19] Miller, D. A. B. *et al.* Electric field dependence of optical absorption near the band gap of quantum-well structures. *Physical Review B* **32**, 1043–1060 (1985).

[20] Fang, K. & Fan, S. Controlling the flow of light using the inhomogeneous effective gauge field that emerges from dynamic modulation. *Physical Review Letters* **111**, 203901 (2013).

[21] Rodriguez, S. R. K. *et al.* Interaction-induced hopping phase in driven-dissipative coupled photonic microcavities. *Nature Communications* **7**, 11887 (2016).

[22] Steger, M., Gautham, C., Snoke, D. W., Pfeiffer, L. & West, K. Slow reflection and two-photon generation of microcavity exciton–polaritons. *Optica* **2**, 1–5 (2015).

[23] Hafezi, M., Lukin, M. D. & Taylor, J. M. Non-equilibrium fractional quantum Hall state of light. *New Journal of Physics* **15**, 063001 (2013).

[24] Umucalilar, R. O. & Carusotto, I. Fractional quantum Hall states of photons in an array of dissipative coupled cavities. *Physical Review Letters* **108**, 206809 (2012).

[25] Amo, A. *et al.* Superfluidity of polaritons in semiconductor microcavities. *Nature Physics* **5**, 805–810 (2009).

[26] Ferrier, L. *et al.* Polariton parametric oscillation in a single micropillar cavity. *Applied Physics Letters* **97**, 031105 (2010).

[27] Ferrier, L. *et al.* Interactions in confined polariton condensates. *Physical Review Letters* **106**, 126401 (2011).

[28] Nalitov, A. V., Solnyshkov, D. D. & Malpuech, G. Polariton z topological insulator. *Physical Review Letters* **114**, 116401 (2015).

[29] Karzig, T., Bardyn, C.-E., Lindner, N. H. & Refael, G. Topological polaritons. *Physical Review X* **5**, 031001 (2015).

[30] Cristofolini, P. *et al.* Coupling quantum tunneling with cavity photons. *Science* **336**, 704–707 (2012).

[31] Imamoglu, A. Inhibition of spontaneous emission from quantum-well magnetoexcitons. *Physical Review B* **54**, R14285–R14288 (1996).

Acknowledgements The Authors acknowledge many insightful discussions with Iacopo Carusotto. This work is supported by SIQURO, NCCR QSIT and an ERC Advanced investigator grant (POLTDES).

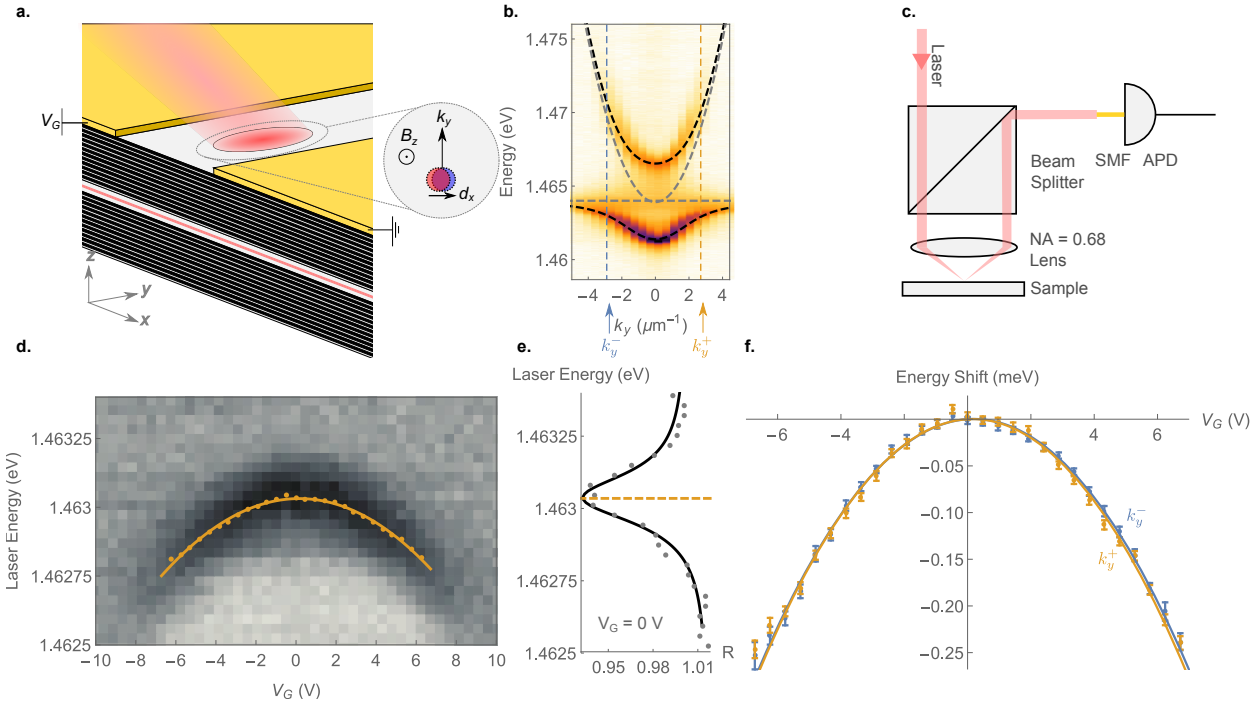

Figure 1: **Description of the sample and characterization experiments at $B_z = 0$ T. a.** The sample, held at 4 K in a helium bath cryostat, contains three 9.6 nm-thick $In_{0.04}Ga_{0.96}As$ QWs located at an antinode of a cavity formed by two distributed Bragg reflectors (DBR). On the sample surface two metal gates are deposited with a 30 μm gap (see Supplementary Information). An electric potential V_G applied to the gates creates an electric field in the x direction. Inset: With a magnetic field in the z direction polaritons excited with in plane wavevector k_y exhibit a dipole moment d_x. **b.** k_y resolved photoluminescence spectra at $B_z = 0$ T. The position on the sample is chosen such that for $|\vec{k}| \sim 0$ the detuning of the cavity mode energy from the exciton resonance is less than 0.09 meV (Figure 1b) which is small compared to the exciton cavity coupling strength 5.2 meV. Gray dashed lines show the extracted bare cavity and exciton dispersions, black lines show polariton dispersions (see Supplementary Information for parameters), orange and blue lines correspond to $k_y = k_y^+$ and $k_y = k_y^-$, respectively. **c.** Experimental setup used in reflection measurements. Reflection of a linearly polarized laser beam (< 100 pW) with in-plane wavevector k_y is coupled to a single mode fiber (SMF) and its intensity is detected with an avalanche-photodiode (APD). **d.** Changes in the reflected intensity of a laser beam exciting polaritons with in-plane wavevector k_y^+ as a function of laser energy and V_G. Yellow dots indicate the extracted polariton resonance energies. Note that the polariton signal is missing when large V_G is applied ($V_G > 8$ V) due to the ionization of the exciton. **e.** Line cut of the reflection spectrum at $V_G = 0$ V. Gray points are the measured reflection data, black solid line shows the fitted lineshape (see Supplementary Information). Dashed yellow line indicates the extracted polariton resonance energy. **f.** Change of polariton energy from $V_G = 0$ V, as a function of V_G for polaritons excited with k_y^+ (yellow) and k_y^- (blue) at $B_z = 0$ T, solid lines are fits to second order polynomials (Blue: $1.9 \times 10^{-6}\ V_G - 5.9 \times 10^{-6}\ V_G^2$, Yellow: $2.2 \times 10^{-6}\ V_G - 5.8 \times 10^{-6}\ V_G^2$). Error bars are confidence intervals extracted from fits.

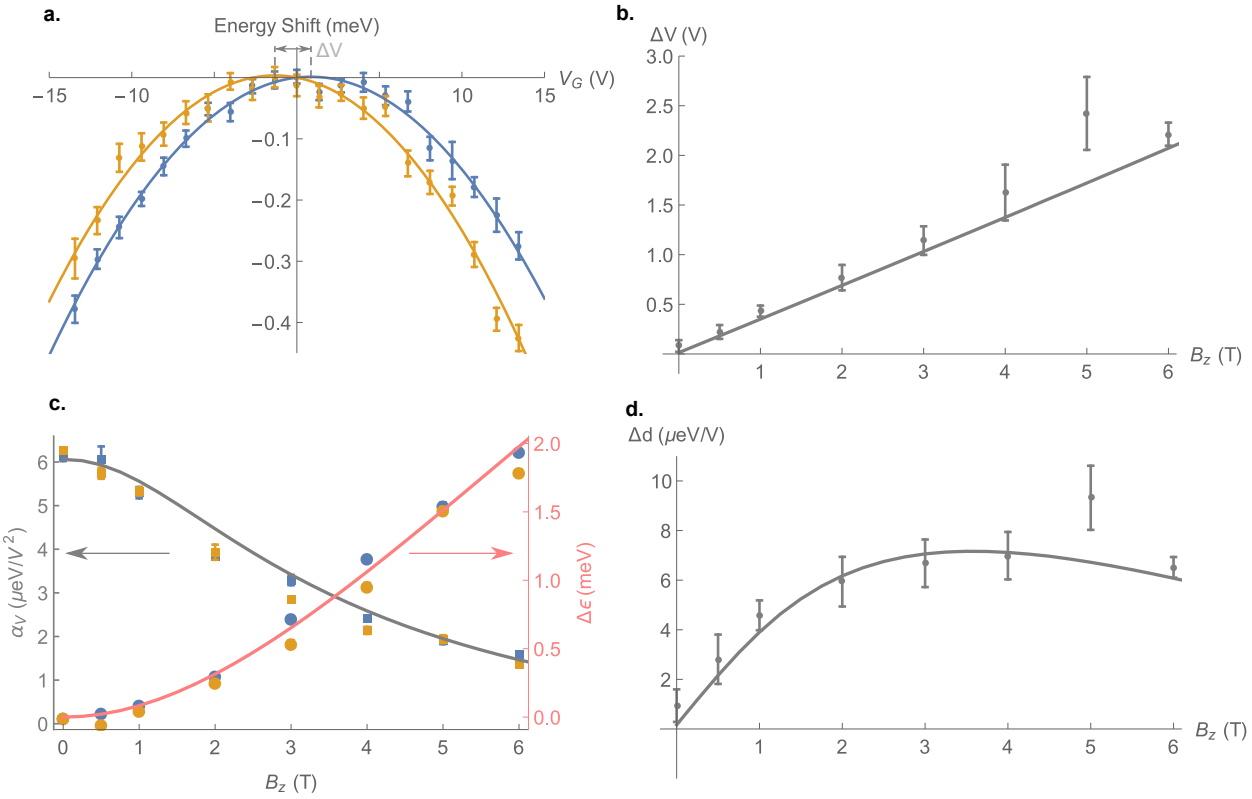

Figure 2: **Magnetic field dependence. a.** Shift of polariton energies with applied voltage for polaritons excited with k_y^+ (yellow) and k_y^- (blue) at $B_z = 5$ T; solid lines are fits to second order polynomials ($-d_V V_G - \alpha_V V_G^2$, Blue: $d_V = 5.2 \times 10^{-6}$ eV/V, $\alpha_V = 1.9 \times 10^{-6}$ eV/V^2, Yellow: $d_V = -3.0 \times 10^{-6}$ eV/V, $\alpha_V = 1.8 \times 10^{-6}$ eV/V^2). Error bars are confidence intervals extracted from fits to the reflection line shape. Gray dashed lines indicate the voltage at which maximum energy occurs for the two parabolas, the gray arrow indicates the difference between them (ΔV). **b.** Using data such as **a** at different B_z, difference between the extracted voltage (ΔV) at which maximum energy occurs for k_y^- and k_y^+ excitations. **c.** Change in α_V (polarizability) with B_z (filled squares, left axis, and gray curve). Change of lower polariton resonant energy with B_z at $V_G = 0$ V (filled circles, right axis, and red curve) from the value at $B_z = 0$ T. Yellow and blue data points are data for k_y^+ and k_y^-, respectively. **d.** Difference between extracted d_V values (electric dipole moment) for polaritons propagating with k_y^+ and k_y^-. For **b** – **d**, error bars are the estimated standard deviations of the mean for three repetitions of the experiment, and the solid lines are results of a numerical calculation (see text and the Supplemental information).

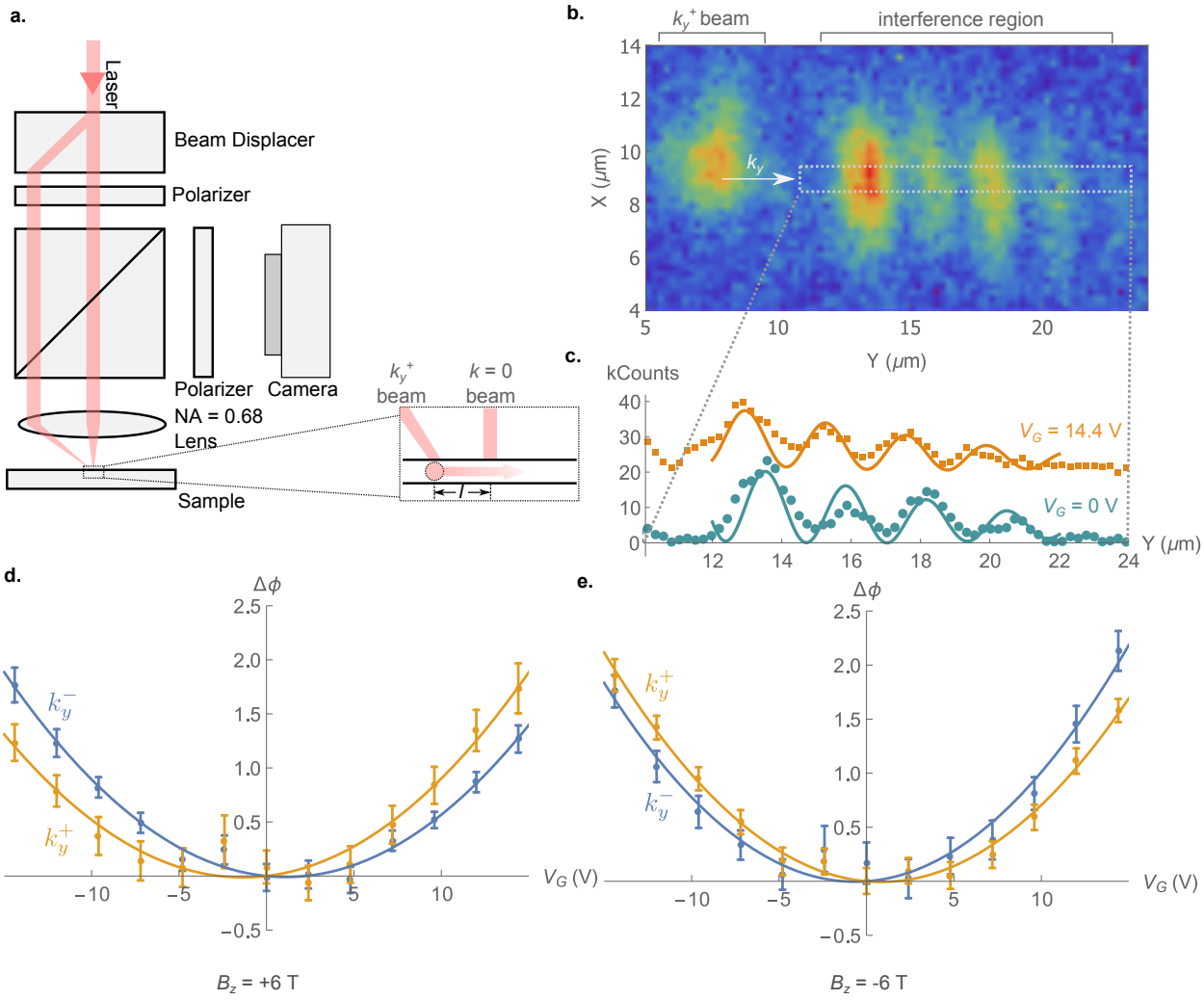

Figure 3: **Demonstration of effective gauge potential for propagating polaritons. a.** A single laser beam is split into two using a birefringent beam displacer, ensuring the relative phase between the two beams do not fluctuate during the experiment. Resulting two linearly polarized beams (total power 40 nW) are incident at different positions on the high numerical aperture (NA = 0.68) lens. One beam that is 1.2 mm off from the center of the lens is incident on the sample with $k_y^{\pm}$. The second beam passes through the center of the lens and thus has vanishing in-plane momentum ($k = 0$ beam). The sample–lens distance is less than the focal length of the lens to ensure that the two beams are incident on the sample with their centers displaced by $l \sim 9\,\mu$m. To detect polariton flow we use an additional linear polarizer between the camera and sample that transmits light that is nearly orthogonally polarized to the incident beams. **b**. An interference image obtained at $B_z = -6$ T, $V_G = 0$ V. Polaritons excited by the k_y^+ beam at 1.46467 eV propagate in the direction indicated by the white arrow. In the spatial region where photons emitted by propagating polaritons overlap with the reflected $k = 0$ beam an interference pattern is observed. **c.** In green, sum of the detected intensity of the interference pattern shown in **b** in the range $x = [8.5 - 9.4]\,\mu$m. In yellow, same as for green but shifted in intensity, for an image obtained at $V_G = 14.4$ V. Solid lines are fits to the model described in Methods and show a difference in the extracted phase. **d.** Change in the extracted phase at $B_z = 6$ T as a function of V_G for polaritons excited with k_y^+ (yellow) and k_y^- (blue). Solid lines show second order polynomial fits to the phase change as a function of V_G (Blue: $-0.016\,V_G + 0.0072\,V_G^2$, Yellow: